Advances in Nano Research, *Vol. 18, No. 4 (2025) 369-380*
https://doi.org/10.12989/anr.2025.18.4.369

Strength behavior and microstructural properties of engineered geopolymer composites reinforced with fiber and carbon nanotubes

Nejib Ghazouani[1a], Abdellatif Selmi[*2], Zeeshan Ahmad[**3] and Nabil Ben Kahla[4,5b]

[1]*Mining Research Center, Northern Border University, Arar 73222, Arar, Saudi Arabia*
[2]*Prince Sattam Bin Abdulaziz University, College of Engineering, Department of Civil Engineering, Alkharj, 11942, Saudi Arabia*
[3]*Department of Civil Engineering, Quaid-e-Azam College of Engineering and Technology (QCET) Sahiwal 57000, Pakistan*
[4]*Department of Civil Engineering, College of Engineering, King Khalid University, PO Box 394, Abha 61411, Saudi Arabia*
[5]*Center for Engineering and Technology Innovations, King Khalid University, Abha 61421, Saudi Arabia*

(*Received August 22, 2024, Revised March 7, 2025, Accepted March 10, 2025*)

Abstract. The main binder in concrete, which is extensively employed in building, Portland cement, is condemned for having a major negative environmental impact. In the field of civil engineering, engineered geopolymer composites (EGC) are a very promising substitute that offers improved sustainability while utilizing comparable special material features to ECC. Environmentally friendly EGC have mechanical properties like traditional Portland cement, however they are susceptible to cracks during tensile and flexural loadings. In this study, polypropylene (PP) fibers and functionalized multi-walled carbon nanotubes (f-MWCNTs) were employed to enhance the ductility of ground granulated blast furnace slag (GGBS)-based EGC (GGBS-EGC). The effect of employing f-MWCNTs and PP fibers was examined by mechanical tests, which comprised single-crack tension assessments, three-point bending, uniaxial tension, and compression tests. The GGBS-based engineering geopolymer showed a peak tensile strength of 3.65 MPa, an elongation of 5.48%, an initial tensile fracture strength of 2.42 MPa, and a compressive strength of 38.03 MPa after 28 days of curing. Having crack widths of 74.56 μm and crack spacings up to 1.43 mm, the classical PSH index for GGBS-EGC2 was 32.67, demonstrating the attainment of saturation multiple cracking and excellent ductility. The production of an amorphous aluminosilicate gel with prominent phases of quartz and calcite was confirmed by Fourier Transform Infrared (FTIR) (FTIR) and X-ray diffraction (XRD) studies, and strong bonding between PP fibers and the matrix was shown by FESEM data. Supplementaryly, f-MWCNTs enhanced the pore structure by lowering detrimental voids.

Keywords: Fourier Transform Infrared (FTIR) spectra; geopolymer composite; MWCNTs; tensile strength; X-ray diffraction (XRD)

1. Introduction

Because Portland cement works so well as a hydraulic binder, it is widely used. However, the process of producing it uses a lot of resources and releases nitrogen oxides, sulfides, and carbides into the environment, which greatly increases carbon emissions. Davidovits introduced the cementitious substance geopolymer in 1978 (Davidovits 1989). This material does not rely on Portland cement. As an eco-friendly substance, geopolymer has generated a lot of controversy these days (Alvee *et al*. 2022, El Ouni *et al*. 2022, Raza *et al*. 2022a, b, 2024a, El Ouni *et al*. 2023). Geopolymers can reduce CO_2 releases by 80% and energy utilization by 60% when equated to cement (Oderji *et al*. 2019). With elongations of up to 6%, engineered cementitious composites (ECC) are well-known for their high tensile strain capacity and strain-hardening tendency (Kamble *et al*. 2014, Khater and Abd El Gawwad 2015, Khater 2016, Farazin and Mohammadimehr 2020, Huang *et al*. 2022, Sokhandani *et al*. 2022). Although ECC meets excellent ductility during tensile stress, cement is the primary raw material employed in the process (Nematollahi *et al*. 2015). Despite maintaining a tensile strength 600 times greater than engineered geopolymer composites (EGC), which use industrial waste as a principal constituent, EGC has mechanical qualities that are equal to those of ECC, according to further research (Artyk *et al*. 2024, Ling *et al*. 2024, Wang *et al*. 2024). There has been a proposal to create improved engineered geopolymers with increased ductility because of the significant vulnerability of EGC to cracking under tensile and flexural loads. The goal of current research has been to develop geopolymers that combine the advantages of EGC and ECC while maintaining ultra-high tensile performance. The ultimate goal is to use these high-tensile geopolymers in place of regular Portland cement.

The main raw materials employed to make geopolymers are industrial wastes, such as fly ash, metakaolin (MK), aluminosilicates like GGBS, and silica fume (SF) (Bayrak *et al*. 2024, Irum and Shabbir 2024, Lao *et al*. 2024, Singh *et al*. 2024). A yearly manufacture of almost 12 million tons

*Corresponding author, Ph.D.,
E-mail: zeeshanlaskani@gmail.com
**Co-corresponding author, Ph.D.,
E-mail: a.salmi@psau.edu.sa
[a] Ph.D., E-mail: nejib.ghazouani@nbu.edu.sa
[b] Ph.D., E-mail: nbohlal@kku.edu.sa

ISSN: 2287-237X (Print), 2287-2388 (Online)

of acidic GGBS is produced by the high-temperature melting of lithium mica (He *et al*. 2018). Amorphous aluminosilicate, which makes up the majority of GGBS and is comparable to fly ash and nano SiO_2, suggests that it may be employed as a cementitious material (Liu *et al*. 2019) In geopolymers, GGBS functions as a bridging agent to stop fracture formation, improving the efficacy of supplementary binders (Karrech *et al*. 2019, Raza *et al*. 2025a). Despite this potential, very little GGBS is employed in construction materials, which leads to serious disposal problems and degradation of the surrounding soil, water supplies, and agriculture. Fortunately, fly ash—one of the most prevalent industrial waste products in China—can be employed as a primary raw material for geopolymers as well as an additive in cement. Fly ash's aluminum oxide and silicon dioxide contents affect its reactivity; the latter is particularly important for the mechanical characteristics and micro-structure of geopolymers. Another industrial waste product is silica fume, which is derived from exhaust gases that are emitted during the refinement of industrial silicon and has a significant concentration of tiny particles. The active ingredient of metakaolin (MK), aluminum silicate, combines with calcium hydroxide in geopolymers to generate C-S-H gel (Alawi Al-Naghi *et al*. 2025a, b, c, Alashker *et al*. 2025, Ahmed *et al*. 2025, Elhadi *et al*. 2024). MK is commonly utilized as a highly reactive mineral additive in geopolymers. Similar to the effects of silica fume, this gel increases the strength and tensile qualities of geopolymers, and over time, its hydration products continue to improve the strength of geopolymers.

According to research, combining the right proportions of CaO and $Ca(OH)_2$ can enhance the compressive strength (CS) of geopolymer composites. After seven days, the CS of the geopolymer with 3% calcium hydroxide increased from 11.80 MPa to 29.20 MPa (Temuujin *et al*. 2009), indicating a notable improvement brought about by the amalgamation of calcium ions. Furthermore, the fabrication and curing times of geopolymers at ambient temperature can be shortened by the amalgamation of calcium ions. It has been discovered that employing water glass (Na_2SiO_3) in the alkaline solution raises the Si/Al ratio in EGC and decreases the permeability of the EGC structure (He *et al*. 2012). The amount of Si-O-Si bonds in the geopolymer gel is increased by the application of alkaline activators. Al-O-Si and Al-O-Al bonds are weaker than Si-O-Si bonds. Therefore, more Si-O-Si bonds result from a greater Si/Al ratio, which improves the CS of geopolymers. Furthermore, gas contamination during the curing stage can be avoided by employing potent alkaline activators to the raw ingredients employed to make geopolymers.

By employing different kinds and quantities of fibers, geopolymers can improve their mechanical qualities, including ductility, tensile elongation, durability, compressive strength, tensile strength, and flexural strength (Khater and Abd El Gawwad 2015, Khater 2016, Jegan *et al*. 2023, Zhang *et al*. 2023, 2024, Chen *et al*. 2024). Long fibers, however, can make geopolymer mixing more difficult since the fibers might not completely dissolve in the alumino-silicate raw ingredients throughout the mixing. Lin *et al*. (2008)'s research indicate that incorporating short fibers into geopolymers is a useful way to enhance their ductility (Lin *et al*. 2008). Building on this, mechanical experiments have been employed to find the ideal fiber blending ratios. Researchers have shown that incorporating fibers with a reduced modulus of elasticity to EGCs results in a decrease in tensile strength but an enhancement in ductility. These hybrid fibers can be PP, steel, PP, or other types of fibers (Raza *et al*. 2024b, c). Researchers discovered that basalt and polypropylene (PP) fibers incorporated into geopolymers resulted in a denser structure as well as a decrease in the amount of free water. The initial reticular structure of geopolymers was not affected by the amalgamation of steel and polypropylene (PP) fibers. These fibers improved the tensile strength of geopolymers in amalgamation to not react with the matrix to create new products. PP fibers have also been discovered to have a reduced modulus of elasticity and high ductility; as a result, samples containing PP fibers in geopolymers show many cracks and great ductility (Lin *et al*. 2008, 2010). Researchers discovered that oxygen, silicon, and aluminum elements combine to form amorphous semi-crystalline materials in both the geopolymers (EGC) and hybrid fibers using energy dispersive X-ray spectroscopy (EDS) study. In the meantime, multi-walled carbon nanotubes have strong CS and Young's modulus. The toughness and mechanical qualities of EGC can be improved by employing nanoparticles, such as carbon nanotubes, nano-silica, nano alumina, etc., according to later research (Aghamohammadi *et al*. 2020, Alomayri *et al*. 2021, Ghazouani *et al*. 2025a, b). The fundamental reason for this enhancement is the advantageous function that functionalized carbon nanotubes have in the geopolymer matrix's micropore structures and interfaces (Abbasi *et al*. 2016). According to Khate, employing multiwalled carbon nanotubes in amounts higher than 0.10% would cause them to become insufficiently dispersed within the geopolymer matrix, which would cause agglomeration and change the micro-structure of the polymers (Khater and Abd el Gawaad 2016).

This study presents a novel approach to enhancing the mechanical performance and durability of GGBS-based engineered geopolymer composites (GGBS-EGC) by optimizing the incorporation of polypropylene (PP) fibers and functionalized multi-walled carbon nanotubes (f-MWCNTs). Unlike previous studies that primarily focus on either mechanical testing or microstructural analysis, this research integrates extensive mechanical evaluations—including uniaxial tensile testing, single-edge notched tensile testing, three-point bending, and compression tests—with advanced microstructural investigations using SEM, XRD, and FTIR. This comprehensive approach provides a detailed understanding of crack-bridging mechanisms and fiber-matrix interactions, establishing a clear correlation between mechanical properties and microstructural evolution. To optimize fiber dosage, an orthogonal experimental design was employed, followed by sample preparation and curing. CS was assessed through uniaxial compression tests, while the impact of Ca^{2+} and f-MWCNTs on strength variation trends was examined. The tensile properties—with strain at break, initial cracking stress, and ultimate tensile strength—were evaluated using uniaxial tensile tests. Fracture energy

Table 1 XRF analysis of raw materials

Chemical composition	SF	MK	FA	GGBS
SiO_2	35.43	51.45	44.09	24.24
CaO	30.21	1.43	7.32	34.67
Al_2O_3	20.54	43.18	26.54	14.32
K_2O	0.54	-	-	2.19
Na_2O	1.54	-	1.54	0.28
Fe_2O_3	0.92	0.8	-	3.87
MgO	7.7	-	2.65	4.53
TiO_2	0.25	1	-	-
SO_3	0.11	-	2.43	7.34
LOI	2.76	2.14	15.43	8.56

Table 2 Features of PP fiber

Property	Value
Length	12 mm
Elongation	4.9%
Aspect ratio	553
Diameter	21.7 μm
Young's modulus	115 GPa
Density	0.97 g/cm³
Nominal tensile strength	>500 MPa

Table 3 Features of f-MWCNTs

Property	Value
Length	5-20μm
Young's modulus	120 GPa
Surface area	160-210 m²/g
Purity	Greater than 95
Outside diameter	10-30 nm
Density	0.06-0.10 g/cm³
Resistivity	< 2100 μΩ.m
Carboxyl content	>0.5 mmol/g

and the contribution of fiber-matrix bridging to ductility were analyzed through bending and notched tensile tests. Finally, microstructural insights obtained from XRD, FTIR, and electron microscopy elucidated the mechanisms responsible for the improved mechanical performance of GGBS-EGC. The findings contribute to the development of highly ductile and environmentally sustainable EGC materials with enhanced load-bearing capacity and fracture resistance, making them promising candidates for advanced structural applications.

2. Materials and methods

2.1 Materials

The chemical composition of four distinct kinds of aluminosilicate raw materials is shown in Table 1. The

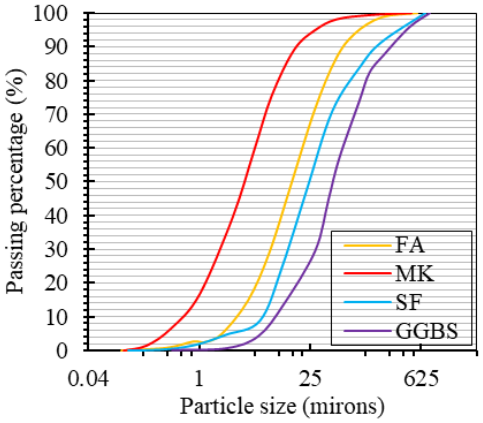

Fig. 1 Sieve analysis of raw materials

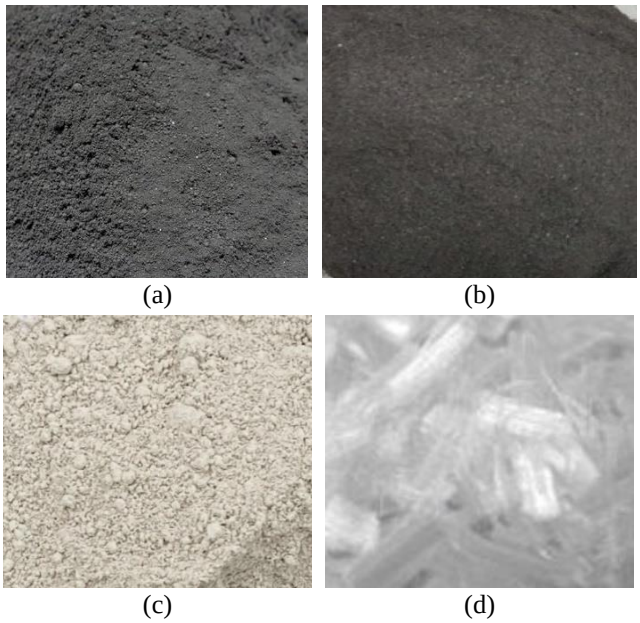

Fig. 2 Raw materials (a) SF (b) GGBS (c) MK (d) PP fiber

distribution of particle sizes for these materials is shown in Fig. 1. Fly ash (FA), which has a high silicon and aluminum content, was used in this investigation. The FA was partially replaced with GGBS. Fig. 2 shows the images of raw materials (SF, GGBS, MK, and PP fiber). GGBS is yellow-brown in color and composed of small particles of sand. Table 2 presents the characteristics of PP fibers. In order to improve their suitability and dispersion in solvents, the selected f-MWCNTs were treated with sulfuric acid to add carboxyl groups. The f-MWCNTs are visible as a powdered black material. Instead of being entirely linear, these nanotubes have a fibrous, extended shape with a small curvature, as shown in Fig. 3 of the SEM analysis utilizing EFSM. Instead of being conical, their ends are usually flat and sealed. The f-MWCNTs have a Young's modulus of 120 GPa and a CS between 60 and 90 GPa. Their main physical characteristics are listed in Table 3. The chosen sodium hydroxide is composed of 8.75% NaO, 27.7% SiO_2, and 63.55% water and has a white, spherical appearance. With a water-to-solid ratio of 1:5 and a modulus ratio of 3.24, it operates as a sodium silicate solution.

Table 4 Variables in orthogonal experiments

Sample ID	PP fiber (vol %)	f-MWCNTs (mass %)	GGBS substitution (mass %)
GGBS-EGC1	0.15	0.05	10
GGBS-EGC2	0.15	0.10	20
GGBS-EGC3	0.15	0.15	30
GGBS-EGC4	0.2	0.05	20
GGBS-EGC5	0.2	0.10	30
GGBS-EGC6	0.2	0.15	10
GGBS-EGC7	0.25	0.05	30
GGBS-EGC8	0.25	0.10	10
GGBS-EGC9	0.25	0.15	20

Table 5 Percentages of ingredients

Ingredient	FA	SF	MK	NaOH	Na_2SiO_3	Quartz sand	Water
Percentage	41%	4%	4%	4%	15%	20%	12%

2.2 Preparation and testing of specimens

To make the alkaline activator, solid, spherical sodium hydroxide with a purity of 99% is first mixed with a Na_2SiO_4 solution having a modulus of 3.24. Using a glass rod, stir this mixture for eight minutes to completely dissolve the sodium hydroxide. After that, the mixture is allowed to reach room temperature and turn clear. By employing a suitable quantity of alkaline activator, the geopolymer's resistance to cracking can be improved. After that, f-MWCNTs and SDS are incorporated into water and properly stirred for a duration of five to six minutes. After that, this mixture is treated with ultrasonication for 30 minutes at 60°C to guarantee that the f-MWCNTs are properly dispersed and functionalized. Next, to create a homogeneous mixture, SF, FA, quartz sand, GGBS, and metakaolin (MK) are incorporated into a mixer and stimulated at a low speed for 3 to 5 minutes. After that, add the prepared alkali to the mixer and stir for a further three minutes. The MWCNTs solution that has been sonicated and functionalized is then incorporated, and it is vigorously agitated for five minutes. Finally, PP fibers are incorporated. After the geopolymer and PP fibers have combined uniformly, the material is put into molds. The room temperature curing was done for the next 28 days.

Orthogonal experiments are conducted using the three dependent variables listed in Table 4 in order to determine the ideal ratio of FA-to-GGBS replacement as well as the ideal ratios of f-MWCNTs and PP fibers for the final geopolymer composition. Three parallel experimental groups are used to assess CS. Six mixes are used for each single-edge notched stress and uniaxial tension test, and four parallel experimental groups are used for the three-point bending tests. Table 5 provides the geopolymer's basic material proportions.

To guarantee correct molding, the slurry is vibrated on a vibrating table at a frequency of 2800 to 3000 cycles per minute after being put into the mold. The compression area of the mold is 40 mm by 40 mm. A CS test is conducted in compliance with national standard GB/T 017671 after a 28-day curing period. The national standard JC/T683 must be followed by the fixture employed in this procedure. Execute uniaxial tensile tests according to JC/T 2641. Fix the dog-bone specimens' ends with fittings, and then install two displacement sensors to track changes in displacement inside the tensile zone with a ±0.001mm measurement precision. Keep the loading rate constant for the test at 0.5 mm/min. A 354 x 75 x 40 mm sample was ready for the three-point bending test. Using a diamond electric drill, a 16.0 mm deep cut was made in the center of the sample's bottom, with the incision pointing down. Using a universal testing machine, which applied a load at a rate of 0.50 mm/min until the sample broke, the matrix fracture energy was ascertained. A saw blade less than 0.6 mm thick was employed to cut a 2 mm deep opening at the middle of the dog-bone specimen's tensile region. In amalgamation, a side incision 6.5 mm deep was made. The experiment was planned with the idea that, throughout the tensile test, only one fracture would occur in order to assess residual energy and peak stress. During the cutting procedure, extra care was taken to ensure that no new cracks developed inside or on the surface of the specimen.

Using a crack measurement tool, ascertain the number and average breadth of cracks in the dog-bone specimen's center 80 mm portion. An optical microscope must be used to inspect the fracture area at a magnification of 150x. To examine the microstructure of GGBS-EGC alumino-silicate raw materials and determine how PP fibers and f-MWCNTs affect tensile performance, use field emission scanning electron microscopy (FESM). Small samples should be taken from the specimens' fracture sites after the tensile tests are completed. These samples should then be placed in a vacuum chamber and dried for 48 hours at 60°C. Next, coat the samples' surfaces with a conductive material, and ninety seconds later, do electron microscopy measurements.

The reaction products of mixes were subjected to X-ray Diffraction (XRD) examination. This involved measuring the angle 2θ, which represents the angle formed by the incident and reflected X-ray beams within the material. Crystalline materials have a regular internal molecular structure, with stable structures usually displaying great intensity. Using the KBr pellet method, FTIR spectroscopy was employed to examine the functional groups and chemical bonds existing in the binders as well as the reaction products of GGBS-EGC. Dried KBr powder (100–200 mg) was carefully mixed with a 0.5 mg sample. In a ball mill, the mixture was processed for one to two minutes. After that, the sample-KBr combination was formed into transparent pellets by pressing it. Ultimately, an infrared spectrometer operating within the designated wavenumber range of 400-4000 cm^{-1} was employed to conduct spectral testing.

3. Results and discussion

3.1 Compressive strength

The best mix of materials—0.15% PP fiber, 0.10% f-

Table 6 Uniaxial tensile test results

Sample ID	Density (kg/m³)	Crack number (80 mm)	Average crack width (mm)	Crack spacing (mm)	First crack strength (MPa)	Ultimate tensile strength (MPa)	Tensile strain capacity (%)	CS (MPa)
GGBS-EGC1	1823.78	28.28	94.36	2.89	0.88	2.38	3.3	26.27
GGBS-EGC2	1664.41	57.57	77.68	1.41	2.44	3.68	5.53	38.41
GGBS-EGC3	1726.16	49.49	84.6	1.65	2.38	3.51	5.18	30.46
GGBS-EGC4	1802.37	34.34	107.41	2.37	0.97	2.81	4.57	35.64
GGBS-EGC5	1750.56	45.45	88.7	1.8	2.16	3.22	4.99	34.18
GGBS-EGC6	1719.19	31.31	92.79	2.61	1.76	3.29	3.6	26.1
GGBS-EGC7	1755.55	48.48	85.52	1.69	1.29	3.15	5.13	24.99
GGBS-EGC8	1803.37	36.36	93.14	2.24	1.33	2.95	4.19	22.59
GGBS-EGC9	1811.32	35.35	89.34	2.31	0.73	2.18	3.91	22.2

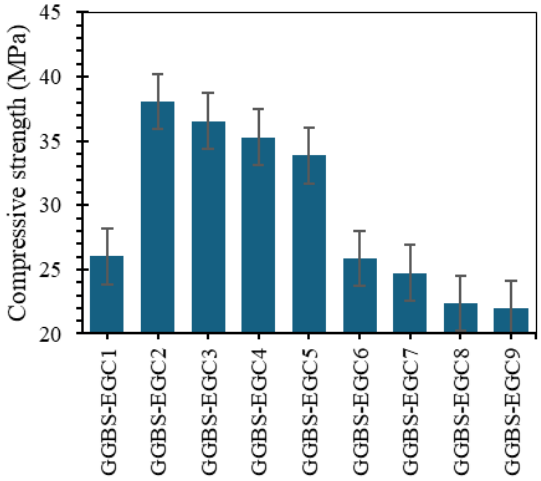

Fig. 4 CS of different mixes

MWCNTs, and 20% GGBS substitution rate—provides 1.16 times the CS of regular Portland cement, with a maximum value of 38.03 MPa. This implies that CS is significantly impacted by substituting GGBS for FA. When applied at a 20% replacement rate, the CaO, silica, and alumina chemicals found in GGBS can decrease the porosity of GGBS-EGC and advance its matrix. Higher material density and strength are a result of this structural enhancement. The reaction of Ca^{2+} in GGBS with alumino-silicates, which forms stable compounds like calcium aluminosilicate and calcium silicate and strengthens GGBS-EGC, is partially responsible for the enhanced CS. Moreover, the alkaline environment's interaction between Ca^{2+} and OH-forms cementitious materials containing calcium and speeds up the nucleation and setting processes. The change of the amorphous N-A-S-H gel into the C-A-S-H and C-S-H gels, which have greater CS than N-A-S-H gel in GGBS-EGC, is also made easier by the presence of Ca^{2+} (García-Lodeiro *et al*. 2011). Fig. 4 shows the values of CS of different mixes. GGBS replacement affects GGBS-EGC's compressive performance more than PP fibers and f-MWCNTs. The CS starts to decrease when the GGBS substitution is more than 20%. This is probably because there is too much Ca^{2+} present, which widens the gap between silica and alumina while also enhancing the synchronization of Ca and O elements. As a result, the interior structure becomes less dense and the chemical stability decreases. When f-MWCNTs are present in ideal numbers, they can scatter uniformly throughout the GGBS-EGC matrix, filling pores and serving as bridges to compact the structure. This results in the most effective compressive performance of GGBS-EGC. On the other hand, too many f-MWCNTs tend to congregate instead of scatter uniformly, which enhances the surface area of the structure and reduces its strength. The fraction of fibers in the GGBS-EGC solution enhances the PP fiber concentration, resulting in a higher specific surface area that improves the bond between the fibers and the matrix and shear flow resistance. Nevertheless, supplementary PP fiber content increases may impede fiber dispersion in the matrix and lead to clumping. This raises the chance of structural failure and the surface area of GGBS-EGC. Consequently, GGBS-EGC obtains its greatest CS augmentation at 0.15% PP fiber content, 0.10% f-MWCNTs content, and 20% GGBS substitution.

3.2 Tensile strength

Stress-strain curves were produced by uniaxial tensile testing of GGBS-based geopolymer that included f-MWCNTs and PP fibers during a 28-day curing period. The stress-strain curve from these tensile tests shows regular changes, as seen in Fig. 5. These variations result from the periodic fluctuations in the stress brought on by the formation of new cracks. Measurements were taken during testing at the point at which the crack first formed and at the point at which the stress and strain reached their ultimate failure. Table 6 provides specifics on the gathered information, such as the number of cracks, average crack width, and maximum elongation. The table shows that GGBS-EGC2 and GGBS-EGC3 have 49 and 57 cracks, individually, with average crack widths of 83.76 μm and 74.56 μm, elongations of 5.13% and 5.48%, and crack spacings of 1.41 mm and 1.62 mm. For every sample, the crack width is less than 110 μm. In GGBS-EGC, smaller cracks signify improved durability. The main ingredient of GGBS-EGC, aluminum silicate, is essential for preventing cracks and supporting external stresses (Lepech and Li 2009). GGBS-EGC2 exhibits greater elongation, initial

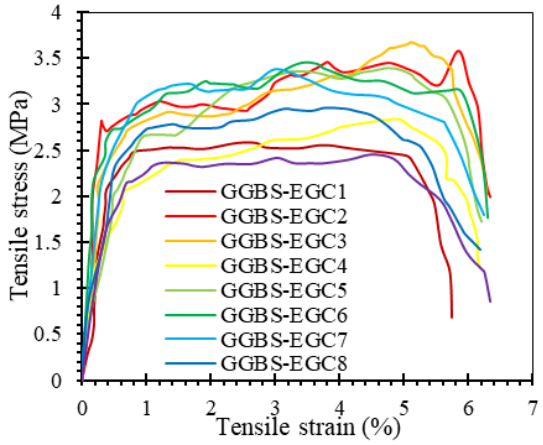

Fig. 5 Stress-strain curve of uniaxial tensile test

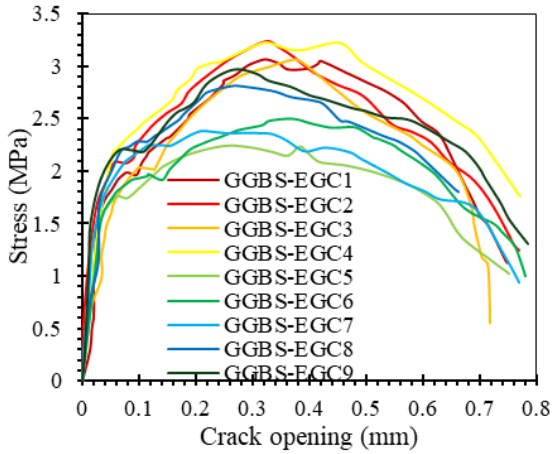

Fig. 6 Single crack tensile test

cracking stress, and ultimate cracking stress in comparison to PP-EGC, indicating that f-MWCNTs enhance GGBS-EGC's tensile strength. Nonetheless, GGBS-EGC2 generally has lower compressive and tensile strengths compared to UHEGC, which is due to the lower reactivity of GGBS (Li *et al*. 2021).

3.3 Bending test and single-crack tensile test

We performed single-edge notched tensile tests and three-point bending tests to ascertain the residual energy from fiber bridging (J_b) and the matrix fracture energy (J_{tip}), which helped to further clarify the remarkable ductility of GGBS-EGC. The stress (σ_{ss}) at the first crack onset must be smaller than the peak tensile stress (σ_B) in the strength requirement for the stress-strain graph of the tensioned matrix to follow both the energy and strength conditions (Leung 1992). The fundamental fiber bridging energy (J_b) in the energy criterion ought to be larger than the fracture energy (J_{tip}). In geopolymer composite materials, the saturation level of numerous fractures is commonly evaluated through the use of the strain hardening exponent (PSH = J_b/J_{tip}) (Kanda and Li 1998). A larger saturation level of cracks is indicated by higher PSH values, which support strain hardening and multiple cracks that are stable (Xu and Reinhardt 1999). According to experimental findings, fiber-reinforced materials can develop saturated multiple cracks if their PSH value is more than 3 (Kanda and Li 2006).

Formulas (1) and (2) can be employed to calculate the matrix's fracture toughness (K_m) (Ohno 2017). It is calculated based on the specimen's mass and dimensions when the three-point bending test reaches its highest load. From uniaxial tensile testing, F_Q stands for the ultimate load, m for the specimen's weight, a for the notch depth, l for the span, t and h for the thickness, and Em for the elastic modulus. The matrix's fracture energy (J_{tip}) is determined by Eq. (3). Eq. (4) computes the residual energy (J_b) from fiber connecting based on stress data, deflection values, and stress-deflection curves acquired from single-crack tension testing. Fig. 6 illustrates crack widening deflection (δ_B) and tensile strength (σ) during single crack tension tests. Notably, GGBS-EGC2 and GGBS-EGC3 show similar curves for crack-widening deflection and tensile strength. The value of σ_B for GGBS-EGC2 and GGBS-EGC3 were 3.41 MPa and 3.17 MPa, respectively. While the value of δ_B for the specimens GGBS-EGC2 and GGBS-EGC3 were 0.306 mm and 0.378 mm, respectively. Table 7 presents $F_Q m$, and K_m values from the three-point bending test. GGBS-EGC2 exhibits a higher $J_b'/J_{tip}/\varepsilon_{t,max}$ value than FA-EGC (Ohno 2017), MFA-EGC (Li *et al*. 2021), and UHEGC2 (Li *et al*. 2021). However, both FA-EGC (Yang *et al*. 2008) and FA-ECC (Yu *et al*. 2015) surpass GGBS-EGC2 in $J_b'/J_{tip}/\varepsilon_{t,max}$ values, indicating potential for improvement in GGBS-EGC2.

However, in tensile testing, GGBS-EGC2 satisfies the strength and energy requirements for strain hardening. Both GGBS-EGC2 and GGBS-EGC3 SHP indices—32.67 and 30.82, respectively—exceed 3, which suggests matrix saturation of multiple cracks. As opposed to GGBS-EGC2 and GGBS-EGC3, the PSH index for MFA-EGC (Li *et al*. 2021) with 1% volume of PP fibers is lower. Reactive sites are incorporated to the matrix by carboxylated multiwalled carbon nanotubes, which encourages the development of polymerization products. Furthermore, in GGBS-based polymers, PP fibers and f-MWCNTs improve bridging capacities at fracture sites under tension, greatly enhancing tensile performance. To sum up, employing PP fibers and f-MWCNTs in polymers based on GGBS significantly improves their ductility (Wu *et al*. 2024).

$$K_m = \frac{(0.5mg \times 10^{-2}) \times a^{0.5} \times l}{t \times h^2} \times 1.5 \times 10^{-3} \times f(a) \quad (1)$$

$$f(a) = \frac{1.99 - \alpha(1-\alpha)(2.7\alpha^2 - 3.93\alpha + 2.15)}{(1+2\alpha)(1-\alpha)^{\frac{3}{2}}}, \quad \alpha = a/h \quad (2)$$

$$J_{tip} = \frac{K_m^2}{E_m} \quad (3)$$

$$J_{tip} \le J_b = \sigma_{B,max} - \int_0^{\delta_B} \sigma_B(\delta) d\delta \quad (4)$$

Table 7 Fracture toughness of GGBS-EGC

Sample ID	Specimen	Peak load (kN)	Mass (kg)	Fracture toughness (MPa/m²)	PSH index and tension strain capacity
GGBS-EGC2	1	2.792	1.834	1.189	$J_{tip}(J/m^2)$ = 31.22
	2	2.762	1.904	1.176	$J_b'(J/m^2)$ = 1017.76
	3	2.642	1.854	1.126	PSH = 32.65
	4	2.732	1.815	1.156	$\varepsilon_{t,max}$ (%) = 5.38
	Average	2.732	1.854	1.162	$J_b'/J_{tip}/\varepsilon_{t,max}$ = 5.94
GGBS-EGC3	1	2.493	1.864	1.063	$J_{tip}(J/m^2)$ = 27.11
	2	2.423	1.825	1.033	$J_b'(J/m^2)$ = 835.61
	3	2.363	1.854	1.007	PSH = 30.79
	4	2.413	1.815	1.028	$\varepsilon_{t,max}$ (%) = 5.12
	Average	2.423	1.844	1.033	$J_b'/J_{tip}/\varepsilon_{t,max}$ = 6.11

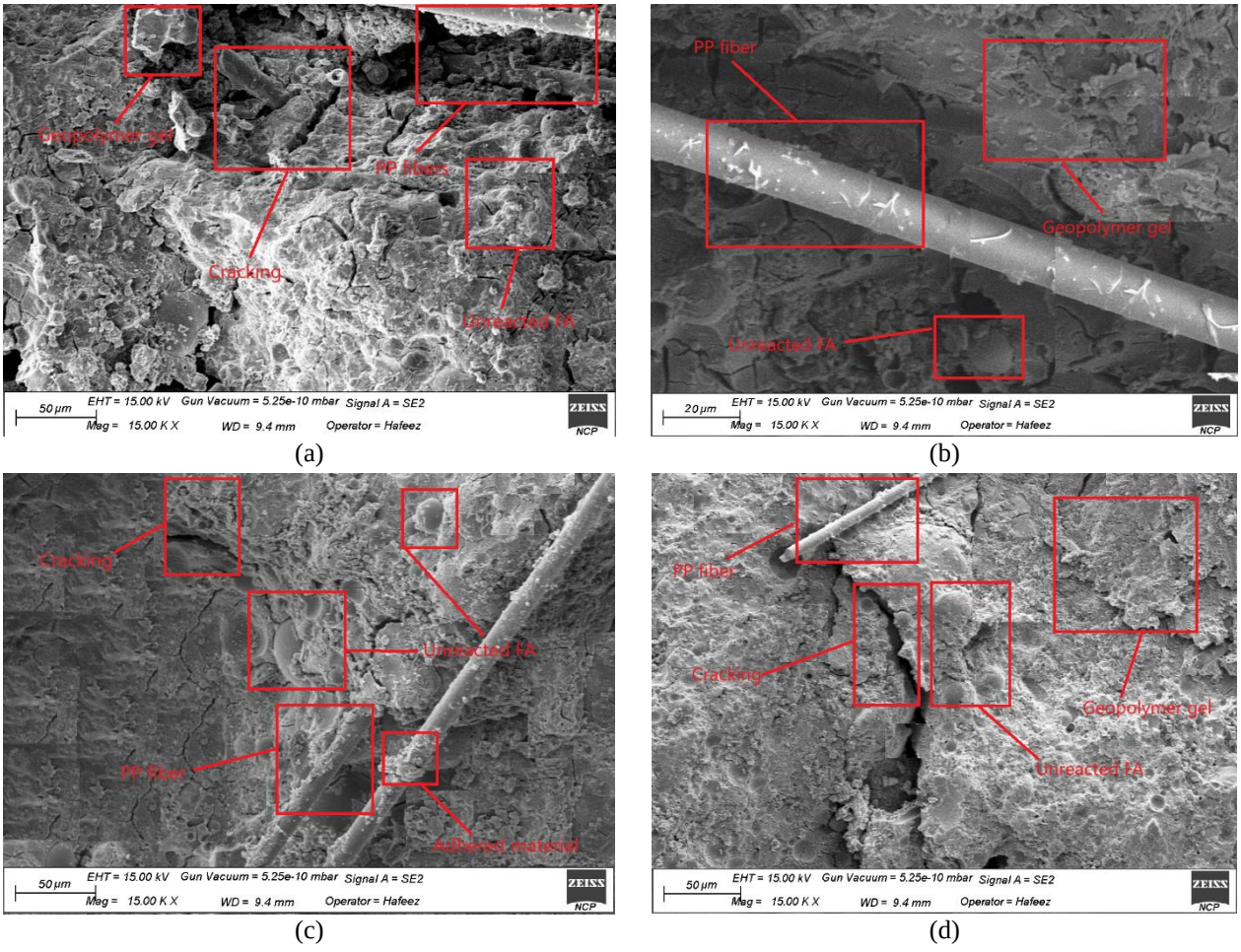

(a) (b) (c) (d)

Fig. 7 FESEM analysis of GGBS-EGC mixes (a) GGBS-EGC2 (b) GGBS-EGC3 (c) GGBS-EGC7 (d) GGBS-EGC9

3.4 Scanning Electron Microscopy (SEM)

The PP fibers and their interaction with the surrounding matrix were examined using the FESEM. When the applied load exceeded the PP fibers' tensile strength, fractures resulted. The extracted PP fibers showed elongated grooves at one end, as shown in Fig. 16(a) and (b), with the other end remaining locked in the matrix. The geological polymer matrix that is still present on the PP fibers in Fig. 7(c) indicates that there is a strong link between them. Because of their great extensibility, the PP fibers play a positive role during tensile stress, as seen in Fig. 7(d), which illustrates how they bridge the matrix. They are able to shift loads and efficiently stop the spread of cracks as a result. Fiber-matrix adhesion is improved and the curing time is shortened when PP fibers are incorporated into the geological polymer solution.

By filling and strengthening the micropores in GGBS-

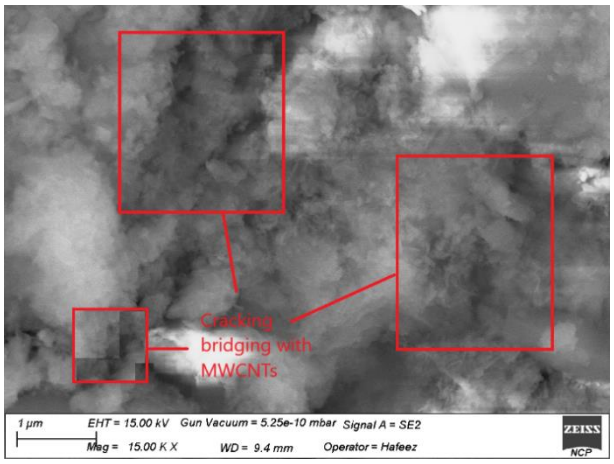

(a)

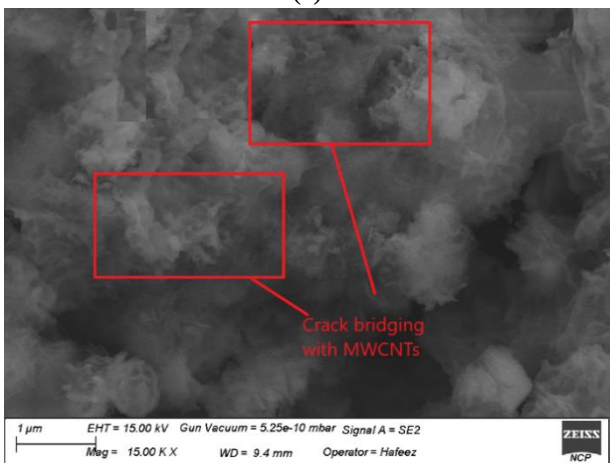

(b)

Fig. 8 FESEM analysis of bridging f-MWCNTs in GGB S-EGC mixes (a) GGBS-EGC2 (b) GGBS-EGC3

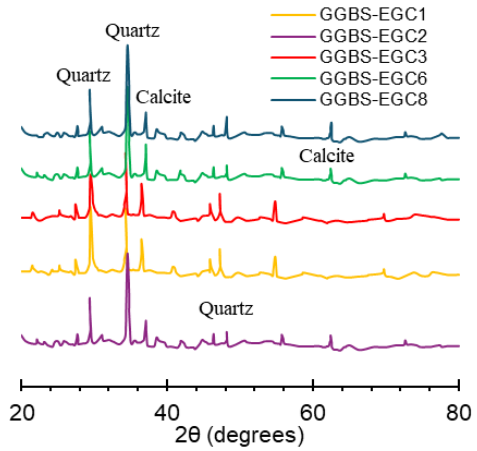

Fig. 9 XRD spectra of GGBS-EGC mixes

EGC, functionalized multi-walled carbon nanotubes (f-MWCNTs) help to enhance the material's CS. On the other hand, an excess of f-MWCNTs could result in matrix clumping, which would reduce the filling effect and perhaps obstruct the entire interaction between the alkaline activator and the aluminosilicate precursors. From a microscopic perspective, f-MWCNTs maximize the pore structure of GGBS-EGC by serving as a bridging and filling agent, minimizing harmful interfaces and lowering the likelihood of fracture development. According to Fig. 8(a), f-MWCNTs work similarly to wires by bridging and drawing GGBS-EGC at microcrack locations to stop the formation of new cracks. By increasing pore density in GGBS-EGC through a nano-filling effect, carboxylated multi-walled carbon nanotubes (f-MWCNTs) improve compressive and tensile strength. With one end remaining implanted in the matrix, several f-MWCNTs are pulled out of crack areas as seen in Fig. 8(b), demonstrating their bridging function within the matrix and their capacity to prevent crack propagation. To sum up, f-MWCNTs and PP fibers play a crucial role in controlling the formation of cracks and enhancing ductility in GGBS-EGC under tensile stress.

3.5 X-ray Diffraction (XRD)

Fig. 9 shows the XRD patterns of some GGBS-EGC mixes. Superior mechanical and crystallinity qualities of the binders and their reaction products are indicated by a greater peak. The main crystalline component in GGBS is gypsum, which has been identified as calcium sulfate. This suggests that GGBS has a high Ca^{2+} concentration. The strength and structure of geological polymers are influenced by the binder material's crystalline phase. The diffraction curves for GGBS-EGC2 and GGBS-EGC3 are primarily flat, indicating a negligible formation of crystalline phases. The quartz crystalline phase, obtained from FA, is represented by the peaks in the 25–30° 2θ range of GGBS-EGC. The GGBS-EGC sample's diffraction peak heights correspond to silica and calcite, with quartz and calcite being the two most common phases. The airborne CO_2 interacts with the alkaline base liquid in GGBS-EGC to produce CO_3^{2-}, which then reacts with the Ca^{2+} in GGBS to form the crystalline phase of calcite. Nevertheless, the amount of calcite crystalline phase in the GGBS-EGC sample is negligible because of the presence of Ca^{2+}, which speeds up the GGBS-EGC setting time, and the alkaline base liquid's quick reaction time with CO_2. By reacting with the binders to generate compounds like sodium silicate and sodium aluminosilicate, the amalgamation of alkali endorses the development of binders (Duxson *et al*. 2006).

3.6 Fourier Transform Infrared Spectroscopy (FTIR)

The use of Fourier-transform infrared (FTIR) spectroscopy is crucial in comprehending the alterations that take place when raw materials are polymerized into geopolymers. The FTIR spectra of some GGBS-EGC mixes are shown in Fig. 10. The main peaks of GGBS-EGC2 and GGBS-EGC3 clearly show a great deal of similarity. The raw materials exhibit vibration frequencies in the 440–490 cm^{-1} range, which are linked to O–Si–O and Si–O–Si bonds. These wavelengths, however, become less pronounced in the reaction products, indicating that the amalgamation of alkali may induce the raw materials to dissolve more gradually, transferring the stretching vibrations to reduced wave-numbers. This change indicates that the raw materials' vibration frequencies under activation have decreased

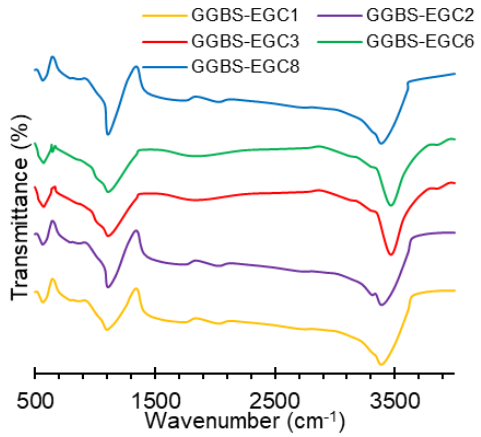

Fig. 10 FTIR spectra of GGBS-EGC mixes

(García-Lodeiro *et al*. 2011). The vibrations mostly correlate to the bending movements of Si-O-Si or Si-O-Al bonds in the range of 570 to 800 cm^{-1}, suggesting the emergence of novel cementitious elements in the geopolymer (Shah *et al*. 2021). This change could indicate that the alkaline activator breaks the O-Si and O-Al bonds on the raw materials' aluminosilicate surface, releasing the ions Al^{3+} and Si^{4+}. As a result, oxygen atoms are shared to form silicon-oxygen and aluminum-silicon tetrahedra, forming Al-O-Si and Si-O-Si connections. Aluminum-silicate oligomers, which might have -Al-O-Si-Si-bonds or -Al-O-Si-Si-Si-bonds, are produced by supplementary interaction between these tetrahedra (Zhuang *et al*. 2016). Amorphous gels such as N-A-S-H, C-A-S-H, and C-S-H develop in the presence of Ca^{2+} and Na^{+} (Zhao *et al*. 2019). Higher calcium concentrations, however, may change the distance between silicon- and aluminum-oxygen tetrahedra, which could affect polymerization and produce a variety of complicated products (Li *et al*. 2021). It is believed that the asymmetric stretching of the Al-O-Si and Si-O-Si bonds is responsible for the vibrations in the 950–1100 cm^{-1} range (Vempati *et al*. 1994). The absorption peak for GGBS in the spectrum is located between 1589 and 1625 cm^{-1}, suggesting the existence of the C=O group, whereas the bending vibration of the H-O-H bond is represented by the peak between 1630 and 1650 cm^{-1} (Li *et al*. 2020). This implies that the GGBS-EGC matrix is where hydration takes place. The infrared wavelength band spanning from 3000 to 3505 cm^{-1} is linked with intensified vibrations of H-O-H bonds, -OH, or moisture present in the surface and pores of the sample (Villa *et al*. 2010). Stronger O-C-O bond vibrations are correlated with absorption in the 1410–1430 cm^{-1} range, which mostly reflects the O–C–O stretching vibrations of the CO_3^{2-} group (Panias *et al*. 2007). The primary cause of these spectrum vibrations in GGBS-EGC is the production of Na_2CO_3 and $CaCO_3$. The O-C-O bond's vibrations match the findings of the XRD research. Different vibrational modes can be employed to uniquely identify the 3D networked matrix that was generated under alkaline circumstances, according to FTIR research (Genge *et al*. 1995). This suggests that the amorphous gel that is produced is an EGC gel that is created when aluminum silicate oligomers copolymerize with Na^{+} and Ca^{2+} ions.

4. Critical discussion

In order to improve mechanical and microstructural qualities, this study emphasizes the possibility of employing PP fibers and f-MWCNTs in GGBS-based engineered geopolymer composites (GGBS-EGC). There were notable gains in compressive resistance, tensile strength, and ductility; however, a few important points need more explanation. The interaction of f-MWCNTs and PP fibers is essential for mechanical performance. Through pore structure refinement, nanoscale load transfer, and improved crack resistance, functionalized MWCNTs enhance strength. However, aggregation makes their dispersion difficult. Although ultrasonic dispersion worked well, for more uniformity, future studies should investigate surfactant-assisted or chemically modified dispersion methods.

Because of its calcium oxide concentration, which encouraged geopolymerization and increased matrix density, GGBS substitution had a considerable impact on CS. However, rheology and workability may be impacted by an excessive amount of GGBS, requiring optimization of the binder proportion. Although changes may be necessary due to variances in raw materials, the 20% replacement level employed in this investigation proved to be ideal. PP fibers' capacity to bridge cracks was essential in improving ductility. Multiple microcracking and strain-hardening behaviors were validated by experimental data. The measured fracture width of 74.56 μm, however, indicates that there is potential for improvement through hybrid fiber combinations or fiber content optimization. Strong interfacial adhesion between PP fibers and the geopolymer matrix was demonstrated by FESEM images; however, more characterization by pull-out tests or nanoindentation is required to measure interfacial strength.

The production of an amorphous aluminosilicate gel with quartz and calcite phases was verified by microstructural investigation using XRD and FTIR. However, endurance issues in harsh conditions are brought up by the matrix's comparatively low crystallinity. To assess long-term performance, future studies should include accelerated durability tests such as freeze-thaw cycles and sulfate resistance. Even though this study offers insightful information on the behavior of GGBS-EGC, more predictive model improvement is necessary to improve the relationship between experimental results and theoretical frameworks. Advanced analytical or numerical modeling methods, including finite element analysis (FEA) or micro-mechanical models, could enhance comprehension of failure processes, stress distribution, and material design optimization.

5. Conclusions

This work successfully combined PP fibers and f-MWCNTs to create a highly ductile GGBS-EGC. Four mechanical tests were employed to evaluate the engineering geopolymer with GGBS. It was discovered that the ideal ratios for f-MWCNTs and PP fibers were 0.1% and 0.15%, respectively. GGBS-EGC was subjected to FTIR and XRD analysis, and field-emission scanning electron microscopy

(FESEM) was employed to look at the matrix surface microstructure. The key findings are as follows:

• After 28 days, GGBS-EGC exhibited a CS of 38.03 MPa, initial tensile fracture strength of 2.42 MPa, peak tensile strength of 3.65 MPa, and 5.48% elongation. The uniaxial tensile test confirmed plastic behavior, with crack spacing up to 1.43 mm and an average crack width of 74.56 μm, staying below 110 μm across all samples.

• The SHP index of 32.67, obtained via SENT and three-point bending tests, confirmed multiple cracking and strain-hardening behavior. f-MWCNTs and PP fibers effectively bridged cracks, enhancing tensile strength.

• An amorphous aluminosilicate gel was produced because of the polymerization of aluminum silicate oligomers with Na^+ and Ca^{2+} ions, according to FTIR analysis. This process produced the geopolymer. The diffraction peaks of the GGBS-EGC mix were compatible with quartz and calcite, and the XRD data indicated that minerals such as quartz and illite were not involved in the reaction. The two highlighted phases in the sample were calcite and quartz.

• A strong connection between PP fibers and the EGC matrix was shown by the FESEM investigation. PP fibers made a substantial contribution to ductility, load transmission, and crack management during tensile testing. The pore structure of GGBS-EGC was enhanced by functionalized multi-walled carbon nanotubes, which acted as fillers and bridges and shrunk the size of potentially hazardous spaces.

Acknowledgement

The authors extend their appreciation to the Deanship of Research and Graduate Studies at King Khalid University for funding this work through a Large Research Project under grant number RGP. 2/203/46. The authors extend their appreciation to the Deanship of Scientific Research at Northern Border University, Arar, KSA for funding this research work through the project number "NBU-CRP-2025-2105".

References

Abbasi, S.M., H. Ahmadi, G. Khalaj and B. Ghasemi (2016), "Microstructure and mechanical properties of a metakaolinite-based geopolymer nanocomposite reinforced with carbon nanotubes", *Ceram. Int.*, **42**(14), 15171-15176. https://doi.org/10.1016/j.ceramint.2016.06.080

Aghamohammadi, H., R. Eslami-Farsani and A. Tcharkhtchi (2020), "The effect of multi-walled carbon nanotubes on the mechanical behavior of basalt fibers metal laminates, an experimental study", *Int. J. Adhes. Adhes.*, **98**, 102538. https://doi.org/10.1016/j.ijadhadh.2019.102538

Ahmed, M., Selmi, A., Ghazouani, N., Raza, A. and Mabrouk, A. (2025), "Mechanical and microstructural characterization of molybdenum tailings-, GGBS-and recycled aggregate based-low carbon self-compacting concrete", *Mater. Lett.*, **382**, 137960. https://doi.org/10.1016/j.matlet.2024.137960

Alashker, Y., Selmi, A., Raza, A. and Ghazouani, N. (2025), "Microstructural and thermal characterization of polyethylene and basalt fiber-reinforced natural zeolite-based engineered geopolymer composites", *Mater. Lett.*, **383**, 137984. https://doi.org/10.1016/j.matlet.2025.137984

Alomayri, T., A. Raza and F. Shaikh (2021), "Effect of nano SiO2 on mechanical properties of micro-steel fibers reinforced geopolymer composites", *Ceram. Int.*, **47**(23), 33444-33453. https://doi.org/10.1016/j.ceramint.2021.08.251

Alvee, A.R., R. Malinda, A.M. Akbar, R.D. Ashar, C. Rahmawati, T. Alomayri, A. Raza and F.U.A. Shaikh (2022), "Experimental study of the mechanical properties and microstructure of geopolymer paste containing nano-silica from agricultural waste and crystalline admixtures", *Case Stud. Constr. Mater.*, **16**, e00792. https://doi.org/10.1016/j.cscm.2021.e00792

Al-Naghi, A.A.A., Ghazouani, N., Selmi, A., Raza, A. and Ahmed, M. (2025a), "Mechanical and microstructural characterization of recycled aggregate geopolymer concrete having high strength and recycled tire steel wire fibers", *Mater. Lett.*, **381**, 137787. https://doi.org/10.1016/j.matlet.2024.137787

Al-Naghi, A.A.A., Ghazouani, N., Selmi, A., Alashker, Y. and Raza, A. (2025b), "Combined effects of elevated temperature, sulfates and chlorides on performance of fly ash and metakaolin-based recycled aggregate geopolymer concrete", *J. Build. Eng.*, **99**, 111561. https://doi.org/10.1016/j.jobe.2024.111561

Al-Naghi, A.A.A., Alashker, Y., Ghazouani, N., Selmi, A. and Raza, A. (2025c), "Mechanical and microstructural characteristics of fly ash-based concrete having copper-zinc oxide and graphitic carbon nitride hybrid composites", *Mater. Lett.*, **383**, 137986. https://doi.org/10.1016/j.matlet.2025.137986

Artyk, Z., Y. Kuan, D. Zhang, C.S. Shon, C.M. Ogwumeh and J. Kim (2024), "Development of engineered geopolymer composites containing low-activity fly ashes and ground granulated blast furnace slags with hybrid fibers", *Constr. Build. Mater.*, **422**, 135760. https://doi.org/10.1016/j.conbuildmat.2024.135760

Bayrak, B., H.G. Alcan, M. Tanyıldızı, G. Kaplan, S. İpek, A.C. Aydın and E. Güneyisi (2024), "Effects of silica fume and rice husk ash contents on engineering properties and high-temperature resistance of slag-based prepacked geopolymers", *J. Build. Eng.*, **92**, 109746. https://doi.org/10.1016/j.jobe.2024.109746

Chen, K.Y., Y.Q. Wang, W.L. Min, J.J. Chen, R.J. Wu, Y. Peng, Y.X. Zhao and J. Xia (2024), "Performance characteristics of micro fiber-reinforced ambient cured one-part geopolymer mortar for repairing", *Constr. Build. Mater.*, **415**, 135086. https://doi.org/10.1016/j.conbuildmat.2024.135086

Davidovits, J. (1989), "Geopolymers and geopolymeric materials", *J. Therm. Anal.*, **35**, 429-441. https://doi.org/10.1007/BF01904446

Duxson, P., J. Provis, G. Lukey, J. Van Deventer, F. Separovic and Z. Gan (2006), "39K NMR of free potassium in geopolymers", *Ind. Eng. Chem. Res.*, **45**(26), 9208-9210.

El Ouni, M.H., A. Raza, H. Haider, M. Arshad and B. Ali (2022), "Enhancement of mechanical and toughness properties of carbon fiber-reinforced geopolymer pastes comprising nano calcium oxide", *J. Australian Ceram. Soc.*, 1-13. https://doi.org/10.1007/s41779-022-00764-9

El Ouni, M.H., A. Raza, H. Haider, M. Arshad, M. Azab and A.B. Elhag (2023), "Behavior of alkali-activated coal ash basalt fiber-reinforced geopolymer nanocomposite incorporated with nano sodium oxide", *Mater. Lett.*, **335**, 133850. https://doi.org/10.1016/j.matlet.2023.133850

Elhadi, K.M., Raza, A., Ghazouani, N., Yaqub, M. and Mabrouk, A. (2025), "Material characterization of high-ductility geopolymer composites developed with industrial and construction & demolition wastes", *Mater. Lett.*, **382**, 137961. https://doi.org/10.1016/j.matlet.2024.137961

Farazin, A. and M. Mohammadimehr (2020), "Nano research for

investigating the effect of SWCNTs dimensions on the properties of the simulated nanocomposites, a molecular dynamics simulation", *Adv. Nano Res.*, **9**(2), 83-90. https://doi.org/10.12989/anr.2020.9.2.083

García-Lodeiro, I., A. Palomo, A. Fernández-Jiménez and D. Macphee (2011), "Compatibility studies between NASH and CASH gels. Study in the ternary diagram Na2O–CaO–Al2O3–SiO2–H2O", *Cement Concr. Res.*, **41**(9), 923-931. https://doi.org/10.1016/j.cemconres.2011.05.006

Genge, M.J., A.P. Jones and G.D. Price (1995), "An infrared and Raman study of carbonate glasses, implications for the structure of carbonatite magmas", *Geochimica et Cosmochimica Acta* **59**(5), 927-937. https://doi.org/10.1016/0016-7037(95)00010-0

Ghazouani, N., Salmi, A., Raza, A., Elhag, A. B., Shabbir, F. and Zahra, F. (2025a), "Mechanical strength and mineralogical properties of fiber-reinforced geopolymer composites with multi-walled carbon nanotubes", *Mater. Lett.*, **382**, 137843. https://doi.org/10.1016/j.matlet.2024.137843

Ghazouani, N., Raza, A. and Elhag, A.B. (2025b), "Synergistic effects of SMA fibers and fly ash on the material characterization of recycled aggregate concrete", *Mater. Lett.*, **379**, 137670. https://doi.org/10.1016/j.matlet.2024.137670

He, J., J. Zhang, Y. Yu and G. Zhang (2012), "The strength and microstructure of two geopolymers derived from metakaolin and red mud-fly ash admixture, A comparative study", *Constr. Build. Mater.*, **30**, 80-91. https://doi.org/10.1016/j.conbuildmat.2011.12.011

He, Z.H., S.G. Du and D. Chen (2018), "Microstructure of ultra high performance concrete containing lithium slag", *J. Hazard. Mater.*, **353**, 35-43. https://doi.org/10.1016/j.jhazmat.2018.03.063

Huang, S.J., S. Kannaiyan and M. Subramani (2022), "Effect of nano-Nb2O5 on the microstructure and mechanical properties of AZ31 alloy matrix nanocomposites", *Adv. Nano Res.*, **13**(4), 407-416. https://doi.org/10.12989/anr.2022.13.4.407

Irum, S. and F. Shabbir (2024), "Performance of fly ash/GGBFS based geopolymer concrete with recycled fine and coarse aggregates at hot and ambient curing", *J. Build. Eng.*, **95**, 110148. https://doi.org/10.1016/j.jobe.2024.110148

Jegan, M., R. Annadurai and P.K. Rajkumar (2023), "A state of the art on effect of alkali activator, precursor, and fibers on properties of geopolymer composites", *Case Stud. Constr. Mater.*, **18**, e01891. https://doi.org/10.1016/j.cscm.2023.e01891

Kamble, V., G. Kodwani, R. Sridharkrishna and B. Ankamwar (2014), "Synthesis of anisotropic defective polyaniline/silver nanocomposites", *Adv. Nano Res.*, **2**(2), 111. https://doi.org/10.12989/anr.2014.2.2.111

Kanda, T. and V.C. Li (1998), "Multiple cracking sequence and saturation in fiber reinforced cementitious composites", *Synopsis*, **9**(2), 19-33.

Kanda, T. and V.C. Li (2006), "Practical design criteria for saturated pseudo strain hardening behavior in ECC", *J. Adv. Concr. Technol.*, **4**(1), 59-72. https://doi.org/10.3151/jact.4.59

Karrech, A., M. Dong, M. Elchalakani and M. Shahin (2019), "Sustainable geopolymer using lithium concentrate residues", *Constr. Build. Mater.*, **228**, 116740. https://doi.org/10.1016/j.conbuildmat.2019.116740

Khater, H. (2016), "Nano-Silica effect on the physicomechanical properties of geopolymer composites", *Adv. Nano Res.*, **4**(3), 181. https://doi.org/10.12989/anr.2016.4.3.181

Khater, H. and H. Abd el Gawaad (2016), "Characterization of alkali activated geopolymer mortar doped with MWCNT", *Constr. Build. Mater.*, **102**, 329-337. https://doi.org/10.1016/j.conbuildmat.2015.10.121

Khater, H. and H. Abd El Gawwad (2015), "Effect of firing temperatures on alkali activated Geopolymer mortar doped with MWCNT", *Adv. Nano Res.*, **3**(4), 225. https://doi.org/10.12989/anr.2015.3.4.225

Lao, J.C., R.Y. Ma, L.Y. Xu, Y. Li, Y.N. Shen, J. Yao, Y.S. Wang, T.-Y. Xie and B.-T. Huang (2024), "Fly ash-dominated high-strength engineered/strain-hardening geopolymer composites (HS-EGC/SHGC), influence of alkalinity and environmental assessment", *J. Clean. Prod.*, **447**, 141182. https://doi.org/10.1016/j.jclepro.2024.141182

Lepech, M.D. and V.C. Li (2009), "Application of ECC for bridge deck link slabs", *Mater. Struct.*, **42**, 1185-1195. https://doi.org/10.1617/s11527-009-9544-5

Leung, C. (1992), "Theory of steady state and multiple cracking of random discontinuous fiber reinforced brittle matrix composites", *ASCE J. Eng. Mech.*, **118**, 2246-2264. https://doi.org/10.1061/(ASCE)0733-9399(1992)118:11(2246)

Li, F., L. Liu, Z. Yang and S. Li (2021), "Physical and mechanical properties and micro characteristics of fly ash-based geopolymer paste incorporated with waste Granulated Blast Furnace Slag (GBFS) and functionalized Multi-Walled Carbon Nanotubes (MWCNTs)", *J. Hazard. Mater.*, **401**, 123339. https://doi.org/10.1016/j.jhazmat.2020.123339

Li, F., Z. Yang, A. Zheng and S. Li (2021), "Properties of modified engineered geopolymer composites incorporating multi-walled carbon Nanotubes (MWCNTs) and granulated blast furnace Slag (GBFS)", *Ceram. Int.*, **47**(10), 14244-14259. https://doi.org/10.1016/j.ceramint.2021.02.008

Li, J., P. Lian, S. Huang and L. Huang (2020), "Recycling of lithium slag extracted from lithium mica by preparing white Portland cement", *J. Environ. Manage.*, **265**, 110551. https://doi.org/10.1016/j.jenvman.2020.110551

Li, M., H. Liu, P. Duan, S. Ruan, Z. Zhang and W. Ge (2021), "The effects of lithium slag on microstructure and mechanical performance of metakaolin-based geopolymers designed by response surface method (RSM)", *Constr. Build. Mater.*, **299**, 123950. https://doi.org/10.1016/j.conbuildmat.2021.123950

Lin, T., D. Jia, P. He and M. Wang (2010), "In situ crack growth observation and fracture behavior of short carbon fiber reinforced geopolymer matrix composites", *Mater. Sci. Eng. A*, **527**(9), 2404-2407. https://doi.org/10.1016/j.msea.2009.12.004

Lin, T., D. Jia, P. He, M. Wang and D. Liang (2008), "Effects of fiber length on mechanical properties and fracture behavior of short carbon fiber reinforced geopolymer matrix composites", *Mater. Sci. Eng. A*, **497**(1-2), 181-185. https://doi.org/10.1016/j.msea.2008.06.040

Ling, Y., Y. Tan, Q. Liu, W. Shi and B. Yang (2024), "Bond performance of reinforcing bars in fly ash-based engineered geopolymer composites under uniform and nonuniform corrosion conditions", *Cement Concr. Compos.*, **152**, 105680. https://doi.org/10.1016/j.cemconcomp.2024.105680

Liu, Z., J.X. Wang, L. Li and D.M. Wang (2019), "Characteristics of alkali-activated lithium slag at early reaction age", *J. Mater. Civil Eng.*, **31**(12), 04019312. https://doi.org/10.1061/(ASCE)MT.1943-5533.0002970

Nematollahi, B., J. Sanjayan and F.U. Ahmed Shaikh (2015), "Tensile strain hardening behavior of PVA fiber-reinforced engineered geopolymer composite", *J. Mater. Civil Eng.*, **27**(10), 04015001. https://doi.org/10.1061/(ASCE)MT.1943-5533.0001242

Oderji, S.Y., B. Chen, M.R. Ahmad and S.F.A. Shah (2019), "Fresh and hardened properties of one-part fly ash-based geopolymer binders cured at room temperature, Effect of slag and alkali activators", *J. Clean. Prod.*, **225**, 1-10. https://doi.org/10.1016/j.jclepro.2019.03.290

Ohno, M. (2017), "Green and durable geopolymer composites for sustainable civil infrastructure", PhD Thesis, University of Michigan, U.S.A.

Panias, D., I.P. Giannopoulou and T. Perraki (2007), "Effect of

synthesis parameters on the mechanical properties of fly ash-based geopolymers", *Colloids Surf. A*, **301**(1-3), 246-254. https://doi.org/10.1016/j.colsurfa.2006.12.064

Raza, A., B. Ahmed, M.H. El Ouni and W. Chen (2024a), "Mechanical, durability and microstructural characterization of cost-effective polyethylene fiber-reinforced geopolymer concrete", *Constr. Build. Mater.*, **432**, 136661. https://doi.org/10.1016/j.conbuildmat.2024.136661

Raza, A., Elhag, A.B., Ghazouani, N., Haider, H. and Chen, W. (2025), "Enhanced performance of fiber-reinforced engineered geopolymer composites incorporating blast furnace slag and calcined bauxite residue", *J. Sust. Cement Based Mater.*, 1-19. https://doi.org/10.1080/21650373.2025.2471835

Raza, A., B. Ahmed, M.H. El Ouni, N. Ghazouani and W. Chen (2024b), "Microstructural and thermal characterization of polyethylene fiber-reinforced geopolymer composites", *J. Build. Eng.*, 109904. https://doi.org/10.1016/j.jobe.2024.109904

Raza, A., M. Azab, Z.A. Baki, C. El Hachem, M.H. El Ouni and N.B. Kahla (2022a), "Experimental study on mechanical, toughness and microstructural characteristics of micro-carbon fibre-reinforced geopolymer having nano TiO2", *Alexandria Eng. J.*, **64**, 451-463. https://doi.org/10.1016/j.aej.2022.09.001

Raza, A., M.H.E. Ouni, A. Brahmia and M. Berradia (2022b), "Mechanical performance of geopolymer composites containing nano-silica and micro-carbon fibers", *Arab. J. Sci. Eng.*, 1-12. https://doi.org/10.1007/s13369-022-06574-2

Raza, A., A. Salmi, M.H. El Ouni, F. Shabbir, N. Ghazouani, B. Ahmed, M.R. Ali and A.S. Hendy (2024c), "A comprehensive review on material characterization and thermal properties of geopolymers, potential of various fibers", *Case Stud. Constr. Mater.*, e03519. https://doi.org/10.1016/j.cscm.2024.e03519

Shah, S.F.A., B. Chen, M.R. Ahmad and M.A. Haque (2021), "Development of Cleaner One-part geopolymer from lithium slag", *J. Clean. Prod.*, **291**, 125241. https://doi.org/10.1016/j.jclepro.2020.125241

Singh, R.P., K.R. Vanapalli, K. Jadda and B. Mohanty (2024), "Durability assessment of fly ash, GGBS, and silica fume based geopolymer concrete with recycled aggregates against acid and sulfate attack", *J. Build. Eng.*, **82**, 108354. https://doi.org/10.1016/j.jobe.2023.108354

Sokhandani, N., A.R. Setoodeh, S.M. Zebarjad, K. Nikbin and G. Wheatley (2022), "The influence of nano-silica on the wear and mechanical performance of vinyl-ester/glass fiber nano-composites", *Adv. Nano Res.*, **13**, 97-111. https://doi.org/10.12989/anr.2022.13.1.097

Temuujin, J., R. Williams and A. Van Riessen (2009), "Effect of mechanical activation of fly ash on the properties of geopolymer cured at ambient temperature", *J. Mater. Process. Technol.*, **209**(12-13), 5276-5280. https://doi.org/10.1016/j.jmatprotec.2009.03.016

Vempati, R., A. Rao, T. Hess, D. Cocke and H. Lauer Jr (1994), "Fractionation and characterization of Texas lignite class 'F' fly ash by XRD, TGA, FTIR, and SFM", *Cement Concr. Res.*, **24**(6), 1153-1164. https://doi.org/10.1016/0008-8846(94)90039-6

Villa, C., E.T. Pecina, R. Torres and L. Gómez (2010), "Geopolymer synthesis using alkaline activation of natural zeolite", *Constr. Build. Mater.*, **24**(11), 2084-2090. https://doi.org/10.1016/j.conbuildmat.2010.04.052

Wang, F., J. Ma, Y. Ding, J. Yu and K. Yu (2024), "Engineered geopolymer composite (EGC) with ultra-low fiber content of 0.2%", *Constr. Build. Mater.*, **411**, 134626. https://doi.org/10.1016/j.conbuildmat.2023.134626

Wu, X., Wang, Q., Zhao, P., Wu, C. and Zhu, D. (2024), "Mechanical properties and enhancement mechanism of lithium slag-contained geopolymers reinforced with PVA fibers and functionalized multi-walled carbon nanotubes", *J. Build. Eng.*, **97**, 110977. https://doi.org/10.1016/j.jobe.2024.110977

Xu, S. and H.W. Reinhardt (1999), "Determination of double-K criterion for crack propagation in quasi-brittle fracture, Part II, Analytical evaluating and practical measuring methods for three-point bending notched beams", *Int. J. Fract.*, **98**, 151-177. https://doi.org/10.1023/A:1018740728458

Yang, E.H., S. Wang, Y. Yang and V. C. Li (2008), "Fiber-bridging constitutive law of engineered cementitious composites", *J. Adv. Concr. Technol.*, **6**(1), 181-193. https://doi.org/10.3151/jact.6.181

Yu, J., J. Lin, Z. Zhang and V.C. Li (2015), "Mechanical performance of ECC with high-volume fly ash after sub-elevated temperatures", *Constr. Build. Mater.*, **99**, 82-89. https://doi.org/10.1016/j.conbuildmat.2015.09.002

Zhang, D., Y. Wang, T. Zhang and Q. Yang (2023), "Engineering and microstructural properties of carbon-fiber-reinforced fly-ash-based geopolymer composites", *J. Build. Eng.*, **79**, 107883. https://doi.org/10.1016/j.jobe.2023.107883

Zhang, P., Z. Feng, W. Yuan, S. Hu and P. Yuan (2024), "Effect of PVA fiber on properties of geopolymer composites, A comprehensive review", *J. Mater. Res. Technol.*, **29**, 4086-4101. https://doi.org/10.1016/j.jmrt.2024.02.151

Zhao, X., C. Liu, L. Wang, L. Zuo, Q. Zhu and W. Ma (2019), "Physical and mechanical properties and micro characteristics of fly ash-based geopolymers incorporating soda residue", *Cement Concr. Compos.*, **98**, 125-136. https://doi.org/10.1016/j.cemconcomp.2019.02.009

Zhuang, X.Y., L. Chen, S. Komarneni, C.H. Zhou, D.S. Tong, H.M. Yang, W.H. Yu and H. Wang (2016), "Fly ash-based geopolymer, clean production, properties and applications", *J. Clean. Prod.*, **125**, 253-267. https://doi.org/10.1016/j.jclepro.2016.03.019

CC